Experimental Validation of Decentralized Control for Gust Load Alleviation in a Wind Tunnel

Kolja Michel*, Felix Stalla† and Gertjan Looye‡
Institute of System Dynamics and Control, German Aerospace Center (DLR), 82234 Weßling, Germany

Thomas G. Schmidt§ and Charlotte Hanke¶
Institute of Aeroelasticity, German Aerospace Center (DLR), 37073 Göttingen, Germany

The concept of decentralized control of ailerons for gust load alleviation was validated in a wind tunnel experiment. Decentralized control uses remote electronic units near the ailerons, which measure the acceleration of the wing and are able to run a local control law. The proposed control laws are using the acceleration as an input to calculate aileron deflections to counteract the gust-induced accelerations of the wing. Using a model of the wing in the wind tunnel, these local control laws were designed and optimized according to defined quality criteria. The experimental results show a high reduction of the accelerations by 33.6 %, which in turn leads to a reduction of the wing root bending moment by 34.2 %. Thereby proving the concept of decentralized control from a flight physical point of view and demonstrating its effectiveness in alleviating gust loads.

I. Introduction

To reduce the environmental impact of aircraft, slender wings with ever higher aspect ratio are planned. To this end, it is necessary to reduce the gust-induced structural loads. To achieve this goal, a decentralized control concept for gust load alleviation is being researched. This method - also known as collocated control - has already been applied in other fields for active structural damping [1]. The sensor is placed directly next to the actuator, which enables a reaction directly on site.

Decentralized control is intended to simplify Gust Load Alleviation (GLA) by reducing system complexity. In principle, the idea is that the actuator is installed with a remote electronic unit and thereby gust load alleviation can be achieved without much interaction with the central flight control. In a previous work in project INTELWI, the decentralized control of the ailerons was examined in detail in simulation for a large passenger aircraft [2]. This concept uses so-called remote electronic units (REUs) that are located at the aileron actuators [3]. These are measuring the accelerations, as well as locally running a control law. Thereby, it is possible to react with small delay to gust disturbances by counteracting the deformation-induced acceleration with local control surface deflection.

In the frame of the DLR project oLAF a wind tunnel experiment with a slender, swept wing was planned. The wing is equipped with actuated flaps and acceleration sensors distributed over the wing. A gust generator was installed in front of the wing to generate disturbances. This offered the opportunity to test the concept of decentralized control for GLA from a flight physical point of view. This paper describes the design, implementation and test of the decentralized control. It is structured as follows: Section II presents the concept of the decentralized control and Section III the experimental setup in the wind tunnel. Then, the control design and optimization is described in Section IV, followed by a summary of the preparatory work of the experiment in Section V. Results are presented in Section VI and finally, conclusions are provided in Section VII.

*Research Associate, Department of Aircraft System Dynamics, kolja.michel@dlr.de
†Research Associate, Department of Aircraft System Dynamics, felix.stalla@dlr.de
‡Head of Department, Department of Aircraft System Dynamics, gertjan.looye@dlr.de
§Research Associate, Department Aeroelastic Experiments, tg.schmidt@dlr.de
¶Research Technician, Department Aeroelastic Experiments, charlotte.hanke@dlr.de

II. Concept of Decentralized Control

The concept of decentralized control for gust load alleviation relies on remote electronic units positioned near the aileron actuators. These are equipped with inertial measurement units (IMU) for acceleration measurements and a processing unit. As a result, control laws can be implemented locally on the REU and it is possible to work with a high sampling rate and a low delay. These decentralized control loops are locally counteracting the gust-induced acceleration of the wing by deflecting the corresponding aileron. [3, 4]

This principle of decentralized control, which is also described as collocated control, is already being used for active structural damping [1]. However, it has not yet been applied to aircraft for GLA and is becoming possible with the development of REUs. This concept was studied extensively in simulations with promising results as described in [2].

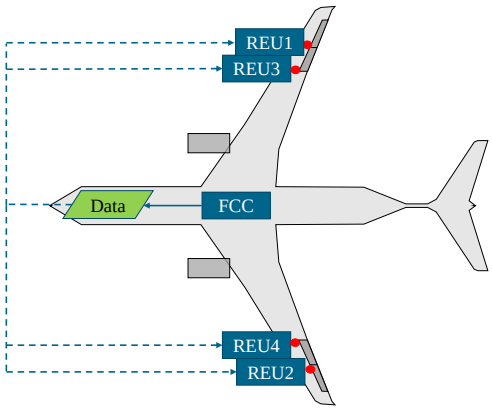

Fig. 1 Concept of decentralized control

Figure 1 shows the concept in simplified form, depicted on an aircraft with a total of four ailerons (two on each side), each equipped with a REU near the actuator. As indicated in the figure, there is no interaction between the REUs and only a small data flow from the Flight Control Computer (FCC). On the one hand, this consists of deflection commands for primary control from the FCC. On the other hand, the expected rigid body accelerations at the REU position are sent to the respective REU. This is subtracted from the values measured by the IMUs in order to avoid the desired rigid body movement being damped by the control system. The aileron command is then calculated on each REU in order to react to the local flexible accelerations. Obviously, this subtraction is not necessary for the wind tunnel experiment, as the wing is fixed and therefore all accelerations are caused by deformation of the wing. The REUs can operate the control at a sampling rate of up to 1000 Hz, which means that the FCC (typically 100 Hz) can be avoided for the fast GLA control loop.

III. Experimental Setup

In the frame of the project oLAF a wind tunnel test campaign with actively controlled surfaces was planned, which offered the opportunity to demonstrate the concept of decentralized control. Although no REUs were available, sensors are located at each control surface, allowing the demonstration of the principle from a flight physical point of view. The experiment was carried out in the low speed wind tunnel in Braunschweig (DNW-NWB). For this purpose, a swept half-wing with a half-span of 1.70 m was mounted in the wind tunnel. The disturbances are generated with a gust generator. Figure 2 shows the experimental setup in the wind tunnel.

The wing is equipped with 5 flaps on the trailing edge and a total of 10 acceleration sensors, two sensors in front of each flap. More information on the design and optimization of the wing can be found in [5]. The wing is mounted on a 6-axes force sensor, to measure for example the wing root bending moment (WRBM). The gust generator is positioned upstream of the wing and consists of fixed symmetrical wing profiles and rotating slotted cylinders, that are capable of generating continuous and discrete gust excitations [6]. In each turn of the cylinder the slot passes twice leading to a gust frequency f_{gust} during continuous gust excitations twice as large as the cylinder rotation frequency. Due to the type of the gust generator also higher harmonics of the gust frequency are excited. The gusts can be measured with the 5-hole probe positioned in the wind tunnel above the wing model. The wind speeds U_∞ used in this experiment were between 30 m/s and 50 m/s.

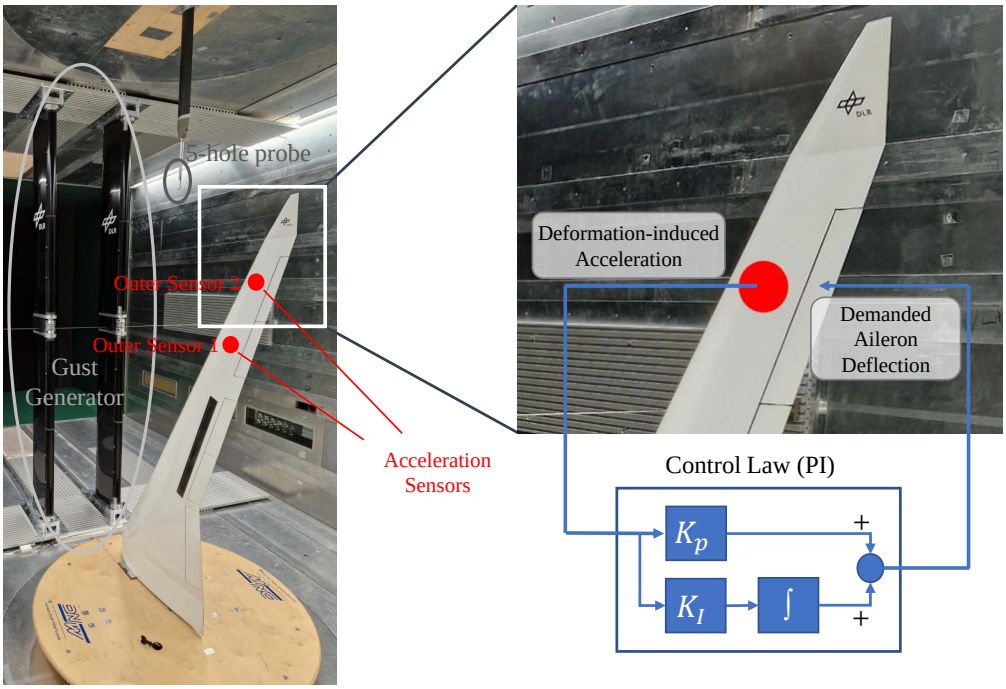

Fig. 2 Experimental setup

Figure 3a shows an impression of the gust angle, measured with the 5-hole probe, of a continuous gust at U_∞ = 30 m/s and a gust frequency f_{gust} = 9 Hz. Figure 3b shows a discrete gust excitation at U_∞ = 30 m/s. For this purpose, the cylinders of the gust generator were rotated at a cylinder rotation frequency of 4.5 Hz by 180° in order to allow only one disturbance to pass through the slot.

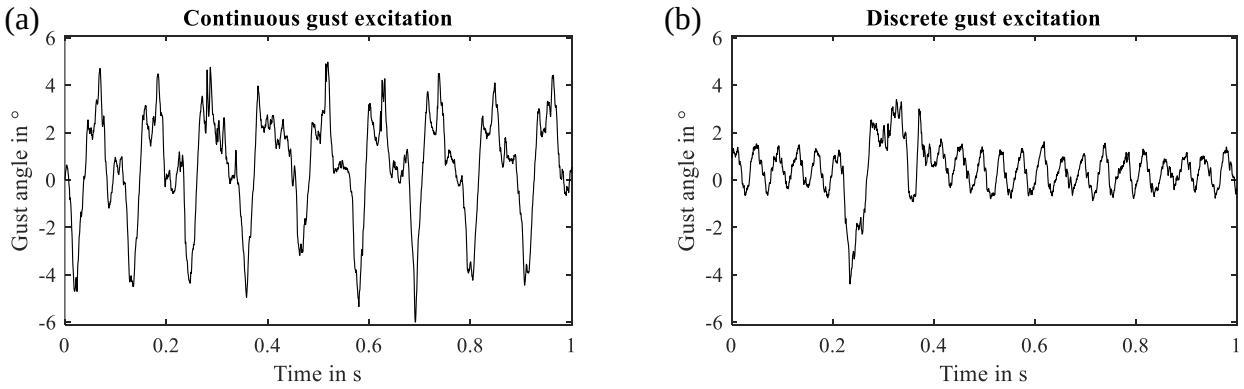

Fig. 3 Continuous and discrete gust excitations at U_∞ = 30 m/s and a cylinder rotation frequency of 4.5 Hz

All the sensor measurements are recorded with a Dewetron data acquisition system [7] with a sampling rate of 3000 Hz. A Jäger ADwin real-time system [8] is also receiving the acceleration data, which then enables active control of the actuators to reduce the gust load. The deformation of the wing is measured via an optical measurement technique, namely Image Pattern Correlation Technique (IPCT) [9]. For this purpose, the lower wing surface is varnished with a dot pattern and the wing is then recorded with two cameras at 100 frames per second. Using image correlation methods, the three-dimensional deformations of the wing can be calculated.

IV. Control Design and Optimization

For the controller design a simulation model is used, which simulates the wing in the wind tunnel under the influence of various disturbances such as gusts. A controller structure is designed for the two outer ailerons, as these are the most effective due to the lever. As well, these are commonly the most reactive flaps on the wing. The acceleration sensor used for the respective aileron is indicated in Fig. 2. Then, the criteria required for the optimization are defined. This results in optimized controller gains, which are then used in the experiment.

A. Modeling

As mentioned, a simulation model of the plant is crucial for model-based control design. This model consists of an aeroelastic model of the wing, combined with an actuator and sensor model, leading to an aeroservoelastic model.

The aeroelastic model is derived using the *VarLoads* framework [10]. As this is a wing model fixed to a wall in a wind tunnel, the calculations for the rigid body motion are not required. These are necessary for a free-flying aircraft. The structural dynamics of the flexible wing are represented in the following equation [11, 12]:

$$\mathbf{M}_{\mathrm{ff}} \cdot \ddot{\mathbf{u}}_{\mathrm{f}} + \mathbf{B}_{\mathrm{ff}} \cdot \dot{\mathbf{u}}_{\mathrm{f}} + \mathbf{K}_{\mathrm{ff}} \cdot \mathbf{u}_{\mathrm{f}} = \mathbf{\Phi}_{\mathrm{gf}}^{T} \cdot \mathbf{P}_{\mathrm{g}}^{\mathrm{ext}}. \tag{1}$$

This second order equation (defined on the f-set) is representing the structural dynamics of the airframe excited by external forces. The structural deformation is described by the modal coordinates $\mathbf{u}_{\mathrm{f}}$, where the number of coordinates is defined to achieve sufficient accuracy for the loads calculation. This results in the modal basis defined in $\mathbf{\Phi}_{\mathrm{gf}}$. The modal properties of the wing are characterized by mass $\mathbf{M}_{\mathrm{ff}}$, damping $\mathbf{B}_{\mathrm{ff}}$ and stiffness $\mathbf{K}_{\mathrm{ff}}$ matrices. The structural matrices originate from a reduced finite element model, derived by static condensation like the Guyan reduction [13]. The design of the wing and the development of this finite element model is explained in [5]. The stiffness properties are determined for condensation points (g-set) along the loads reference axis. The transformations between the condensation points (g-set) and the flexible dynamics are defined by $\mathbf{\Phi}_{\mathrm{gf}}$. The mass distribution of the wing is approximated by uncoupled lumped masses attached to the g-set. External forces and moments $\mathbf{P}_{\mathrm{g}}^{\mathrm{ext}}$ are aerodynamic and gravity induced in the wind tunnel experiment.

The external aerodynamic loads $\mathbf{P}_{\mathrm{g}}^{\mathrm{aero}}$ are modeled by a panel method based on potential flow theory, as it is sufficiently accurate for the low Mach numbers used in the wind tunnel. The Doublet Lattice Method (DLM) [14, 15] is used to obtain the unsteady aerodynamic forces in the frequency domain [10]:

$$\mathbf{P}_{\mathrm{g}}^{\mathrm{aero}}(k) = q_{\infty} \cdot \mathbf{T}_{\mathrm{kg}}^{\mathrm{T}} \cdot \mathbf{S}_{\mathrm{kj}} \cdot \underbrace{\mathbf{Q}_{\mathrm{jj}}(k) \cdot \mathbf{w}_{\mathrm{j}}}_{\Delta \mathbf{c}_{\mathrm{p,j}}(k)}, \tag{2}$$

where q_{∞} is the freestream dynamic pressure and $\mathbf{T}_{\mathrm{kg}}$ is the splining matrix. This matrix maps the displacement of the structural grid to the aerodynamic panel model and, vice versa, the aerodynamic loads to the structural grid. The matrix $\mathbf{S}_{\mathrm{kj}}$ integrates the pressure coefficients $\Delta \mathbf{c}_{\mathrm{p,j}}(k)$ over each panel. The pressure coefficients depend on the Aerodynamic Influence Coefficient (AIC) matrix $\mathbf{Q}_{\mathrm{jj}}(k)$ as well as the downwash $\mathbf{w}_{\mathrm{j}}$. The AIC matrix is derived for multiple reduced frequencies $k = \omega \frac{c_{\mathrm{ref}}}{2U_{\infty}}$ [12].

The downwash $\mathbf{w}_{\mathrm{j}}$ in Eq. (2) is produced by the motion of the wing described by the modal amplitude $\mathbf{u}_{\mathrm{f}}$ and its derivatives, a control surface deflection and its derivatives, or a gust input w^{G}. These inputs are specified as time domain signals, while equation 2 is obtained in the frequency domain. For the transformation to the time domain, the Rational Function Approximation (RFA) called Roger's method [16, 17] is applied for the wing's aerodynamics, while the gust aerodynamics are treated by the Loewner Framework [18, 19].

The standard scenario for the structural load analysis of a atmospheric disturbance encounter is the 1-cos discrete gust encounter defined in the certification standard CS 25.341 [20]. This disturbance wind profile is characterized by

$$\mathbf{w}_{\mathrm{j}}^{G}(t) = \begin{cases} \alpha^{G} \cdot \left(1 - \cos\left(\frac{\pi \cdot \mathbf{x}_{\mathrm{j}}(t)}{H}\right)\right) & t_s \leq t \leq t_e, \\ 0 & \text{otherwise}, \end{cases} \tag{3}$$

where α^{G} is the maximum gust angle in radian, t_s the start time, t_e the end time of the gust encounter, $\mathbf{x}_{\mathrm{j}}$ is the distance in aircraft longitudinal axis between the aerodynamic panel and the reference gust coordinate, and H is the gust

gradient length. Therefore $\mathbf{w}_{\mathrm{j}}^{G}(t)$ contains the disturbance time signal for each individual aerodynamic panel j.

The actuator model is a first order linear transfer function with experimentally identified parameters. The cut-off frequency is at 90 rad/s and there is a actuator dead time of 4.3 ms. The sensor dynamics are represented by a time delay of 1 ms. Together with the delay caused by the controller, this conservatively results in a total delay of 8 ms, which is approximated by a second order Padé element for the linear model. The aeroelastic model together with the actuator and sensor dynamics leads to the aeroservoelastic model of the wing, which is used for the controller optimization.

A more detailed description of the modeling process can be found in [21].

B. Controller structure

The design of a controller offers many degrees of freedom. A suitable controller structure must therefore be selected for the decentralized concept. The controller must be able to run independently on the REUs and should therefore not require too many inputs or be too computationally intensive. As the potential application is in aviation, the safety-specific approval requirements must also be taken into account. In particular, this means that a proven and comprehensible controller structure is used.

Therefore, a controller with proportional part and integral part is used (PI). The controller input is the acceleration signal of the sensor next to the respective aileron. These acceleration signals are subjected to noise as they cannot be ideally measured.

On the right side of Fig. 2 the structure of the controller is shown. The control parameters K_P and K_I can be seen, as well as the output of the controller: the demanded surface deflection (ailerons in this case).

C. Definition of quality criteria

The decentralized control is intended to achieve the highest possible reduction of accelerations on the wing. This also reduces the loads on the wing - such as the wing root bending moment. To achieve this, while considering the limitations of the actuator and the stability of the decentralized gust load alleviation system, quality criteria are defined to evaluate the control. These are the following:

- Maximum z-acceleration near aileron $a_{z,\,ail,\,max}$
- Integral of z-acceleration $Int_{a_{z,\,ail}}$
- Maximum position of aileron δ_{max}
- Maximum rate of aileron $\dot{\delta}_{max}$
- Integral of aileron position Int_{δ}
- Modulus margin Mm for stability

The first two criteria are defined to evaluate the performance of the gust load alleviation control. One is the maximum z-acceleration near the aileron $a_{z,\,ail,\,max}$. Also, its integral over time is defined as criterion $Int_{a_{z,\,ail}} = \int |a_{z,\,ail}|\, dt$. While $a_{z,\,ail,\,max}$ takes the maximum values into account and thus ensures that the control reduces the acceleration peaks during optimization, the criterion $Int_{a_{z,\,ail}}$ ensures that the decay of the accelerations after excitation also takes place in a shorter time.

The performance of the actuator is crucial for gust load alleviation control. Of course, an actuator with unlimited speed is desirable here in order to react quickly to very short-term disturbances (such as gusts). In reality, it is a compromise between weight, economic efficiency and possible gust load reduction, which is why the deflection and speed of the actuator are limited. In order to avoid the decentralized control being constantly in saturation, the limitations of the actuator are already taken into account in the controller design. The maximum position of the aileron δ_{max} and its maximum rate $\dot{\delta}_{max}$ are used as criteria. This type of active control places a very high load on the actuator due to the high activity of the control surfaces. The activity of the actuator is only partially described by the previous two criteria, which is why a further criterion is introduced to express the activity numerically. The integral of the control surface position $Int_{\delta} = \int |\delta|\, dt$ is used for this.

In addition to the criteria mentioned above, the stability of the control loops must always be guaranteed. For this purpose, the modulus margin of the individual controllers is considered.
The modulus margin Mm [22] is a stability criterion that considers the combined amplitude and phase reserve. It

is particularly suitable for optimization as it reduces the number of criteria and offers the optimization algorithm fewer 'loopholes'. If the amplitude and phase reserve are considered separately, there is a possibility that a small gain amplification with a simultaneous phase shift will lead to an unstable controller. This is prevented with the modulus margin. Figure 4 shows a Nyquist plot that can be used to visualize the various stability criteria.

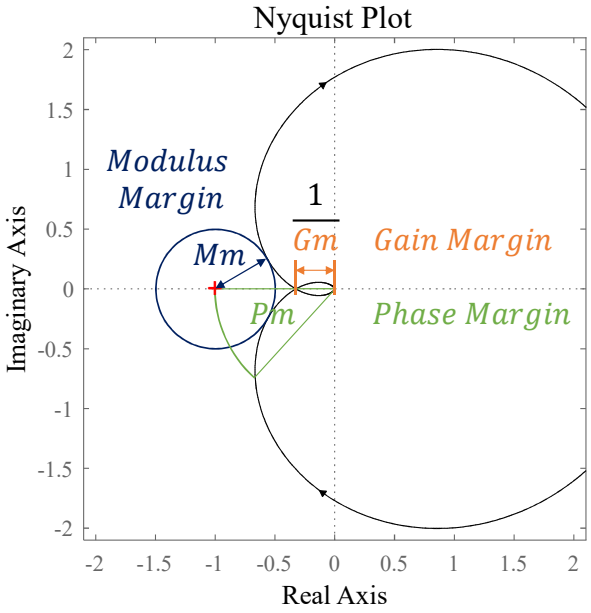

Fig. 4 Nyquist plot with several stability criteria

In Fig. 4 a Nyquist plot (in black) can be seen with the margins for gain and phase. Also shown is the modulus margin, which can be described as the distance of the Nyquist plot from the critical 'instability' point $(-1|0)$. A typical requirement is a modulus margin $Mm > 0.5$.

D. Optimization

The controller gains of the local control loops are optimized with the primary goal of reducing the accelerations of the wing. By reducing the gust-induced accelerations, the wing is deflected less and the structural loads are reduced.

The optimization process was carried out with the DLR-SR tool for Multi-Objective Parameter Synthesis (MOPS) [23]. Therein various optimization algorithms are available, such as gradient-based and genetic algorithms. Optimization results are clearly displayed in parallel coordinates, which are also shown below in Fig. 5. In the optimization the previously defined quality criteria, normalized with the open loop reference value (decentralized control inactive) and given restrictions as actuator limits, are used. Through the normalization, the values must then be reduced below a value of <1 in order to be better than open loop and not violate any restrictions. The modulus margin criterion is defined inversely, so that a value of 1 is shown in the parallel coordinates for a demand value of 0.5 and the value decreases for a larger margin. With an additional change to the demand value, the weighting on certain criteria can be increased. The optimization algorithm then always attempts to reduce the maximum value of the criteria in the various iterations. The optimization is carried out with suitable scenarios such as 1-cos gusts, as already done in previous projects. Even if the gust generator creates gust profiles that deviate from this, it was considered reasonable to adhere to a generally valid controller design methodology. Two different gust length, a short and a long 1-cos gust, are applied in the optimization setup. The controller gains were optimized with a model for a stream velocity of 50 m/s. These were then scheduled with the dynamic pressure to adapt to different wind speeds in the experiment.

The aforementioned representation in Parallel Coordinates helps the evaluating engineer to get a good overview. During the optimization, numerous favourable iterations are plotted, which also makes changes between iterations visible. In Fig. 5 the optimized controller can be seen in Parallel Coordinates. The evaluation for the gust scenario

with the short 1-cos gust is displayed. Blue axes show criteria that are not active but are still relevant for the viewer's assessment. For example, the wing root bending moment, the reduction of which is not the primary objective of the optimization, but a desired consequence of the reduction of the wing accelerations. No modified demand values were used for weighting in the illustration here. For example, additional weightings on the criteria $a_{z,\ ail,\ max}$ and $Int_{a_{z,\ ail}}$ were active during the optimization in order to reduce them further. In the interest of clarity, here these values are only normalized with the open loop reference value or with given restrictions as actuator limits. As can be seen, all criteria are below 1, meaning that all requirements are met in this simulative analysis of the optimized controller.

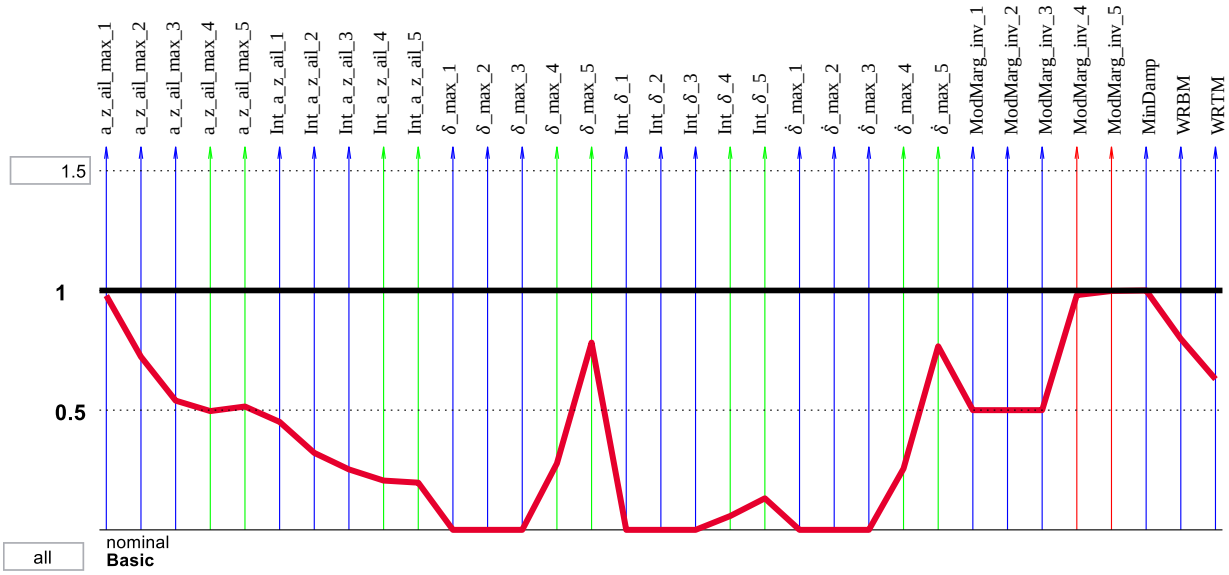

Fig. 5 Parallel Coordinates of the optimized controller

V. Implementation and Preparation of Experiments

This chapter provides a brief overview of the preparatory work for the wind tunnel experiments. It is done without any claim to completeness. However,it should be emphasized that the effort involved in preparing such an experiment should not be underestimated.

Preparatory work was carried out with the wing model outside and inside the wind tunnel. First, the actuators of the control surfaces were put into operation. They are controlled by means of pulse-width modulation (PWM). It turned out that this is quite sensitive and it is important that the controlling Jäger ADwin system and the power supply of the actuators are grounded together.

The Jäger ADwin real-time system and a Dewetron data acquisition system were available to record the sensor data. First, suitable measuring amplifiers had to be selected. Their measurement amplification was also optimized in order to reduce the noise of the sensors. The sign of the measured values was also checked.

In the next step, the 10 sensors distributed across the wing had to be calibrated, as the magnitudes of the measured values were not yet correct. After a manual excitation, the wing oscillated at the frequency of the first bending mode. However, for example sensors closer to the wing root, showed larger values than the sensors at the wing tip. To calibrate the sensors, the wing was excited once in the simulation and on the physical wing model and then allowed to oscillate freely. The data recorded after one second served as the basis for the calibration. The peak-to-peak acceleration values from the simulation served as a reference for the proportions of the various sensors. The measured values from the acceleration sensors were first filtered. Peak-to-peak values averaged from several measurements were the basis for calculating the ratios between the simulation value and the measured value of each sensor. As the two outer sensors

showed comparable values in the expected order of magnitude, one of these sensors was defined as 'correct' and thus given a scaling factor of 1. The scaling factors for the remaining sensors were then calculated together with the ratios. This also showed that two of the sensors delivered measured values of insufficient quality. This may be due to incorrect installation or a defect of the sensor.

Subsequently, the sensor defined as 'correct', which served as a reference for the magnitudes of the sensors, was checked with the IPCT data. For this purpose, the deformation of the wing at the position of the sensor was calculated using the data from the optical measurement method. This deformation can also be determined by double integration of the measured acceleration values. The comparison shows that the two deformation curves hardly differ from each other. Therefore, the sensor defined as 'correct' functions correctly and the calculated scaling factors are retained.

The noise of the acceleration sensors was then regarded, which is not insignificant even when the wing is stationary. It was found that additional vibrations and noise are introduced simply by energizing the actuators and thus setting a constant position. In order to cope with the noise and the offset of the sensors in the control system, suitable filters must be defined. A first-order high-pass filter with a cut-off frequency of 1 Hz ensures that an offset and a slow drift of the signal are filtered out. A first-order low-pass filter with a cut-off frequency of 30 Hz filters out high-frequency noise. The relatively high cut-off frequency is intended to prevent an excessive phase shift in the frequency band in which the controller is to be active. These filters were then also taken into account in the optimization of the final controller.

The controller, which was designed in Matlab Simulink, must then be transferred to the Jäger ADwin real-time system. The controller interfaces (such as sensor inputs and controller outputs) are defined for this purpose. After automatic C code generation, the controller is flashed to the real-time system. In initial tests without wind, it was checked that the flaps deflect in the correct direction when accelerated by manual excitation.

The simulation model was then validated with data of the wing in the wind tunnel. For this purpose, static deflections and sine sweeps were performed with the actuator. More on this can be found in [21].

During the tests in the wind tunnel, it was noticed in high-frequency video recordings that the 5-hole probe was set in oscillation by the gusts. As a result, its data can only be used to a limited extent, for example for a qualitative impression of the gust angle.

Initial controller experiments in the wind tunnel show that the gust-induced accelerations with the gust generator are greater than those of the 1-cos gusts used in the simulation. Therefore, the output of the decentralized controller was reduced to 80 % so that the commanded deflections remain as far as possible within the realizable range. The commanded deflections are nevertheless limited in order to prevent reaching the physical end point.

An important safety function that was implemented in the course of the preparations is switching off the control if the measured acceleration is too high. This is intended to prevent an unstable controller from causing the wing to oscillate to such an extent that it breaks in the worst case.

VI. Results

In this chapter an overview of the wind tunnel experiments with the decentralized control will be given. First, the results for continuous gust excitations are discussed. Then a comparison is made between simulation and experiment, which leads to a better understanding of the controller behavior. Finally, the results for discrete gust excitations are shown.

The following calculation methods are used to calculate the gust load alleviation regarding acceleration and wing root bending moment:

$$GLA_{Acc} = 1 - max\left(\frac{a_{min,\,CL}}{a_{min,\,OL}}, \frac{a_{max,\,CL}}{a_{max,\,OL}}\right),\ GLA_{WRBM} = 1 - \frac{|WRBM|_{max,\,CL}}{|WRBM|_{max,\,OL}}, \tag{4}$$

with the subscript OL for 'open loop' (control inactive) and the subscript CL for 'closed loop' (decentralized control active).

A. Continuous gust excitation

The experiments show that a high reduction in accelerations and loads can be achieved, particularly in the range of excitation close to the natural frequency of the wing (≈ 9 Hz). The highest accelerations of the wing also occur in this range, so it is very useful if these are reduced, as this reduces the maximum stress on the structure.

Figure 6a-c shows acceleration measurements from the experiment with a continuous gust frequency of 9 Hz and the wind speeds 30 m/s, 40 m/s and 50 m/s.

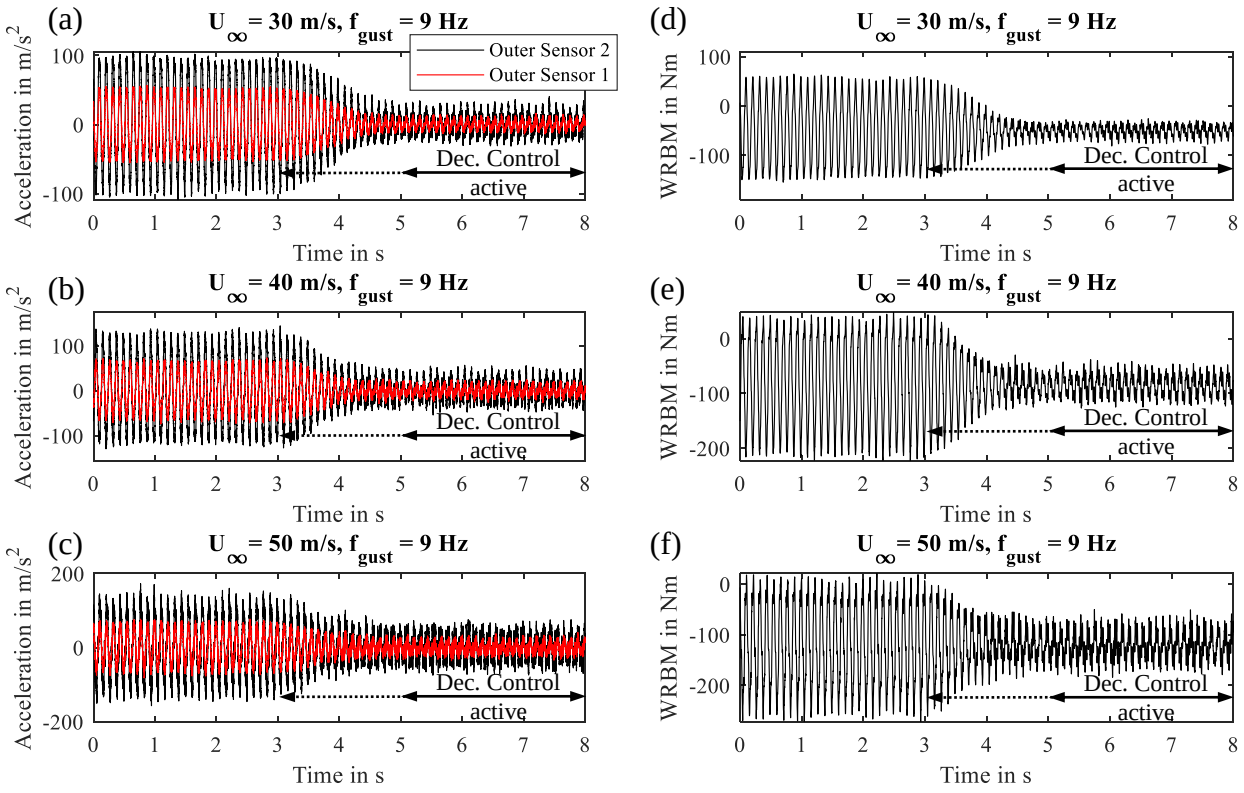

Fig. 6 Acceleration (a-c) and WRBM (d-f) measurements at different wind speeds and gust frequency 9 Hz

The sequence begins with inactive control. The wing is set in oscillation by the continuous gusts. Then, at 3 s, the control for gust load alleviation is gradually (dotted line) activated. After further two seconds, the control is fully active. A high reduction of the accelerations can be seen at the 'Outer Sensor 2', which is located at the height of the outer aileron, as well as at the 'Outer Sensor 1' located near the inner aileron (cf. Fig. 2). The maximum acceleration at a wind speed of 30 m/s is reduced by 60 % with the control. This reduction of the acceleration is slightly less pronounced for higher wind speeds, nevertheless achieving a reduction of 50 % at a wind speed of 50 m/s.

The wing root bending moment, which was recorded with the force sensor at the base of the wing, is shown in Fig. 6d-e for a continuous gust frequency of 9 Hz and the wind speeds 30 m/s, 40 m/s and 50 m/s. At first with inactive control, and then with the control active, as described for the figure before. The wing root bending moment, which is usually a dimensioning factor in the design of the wing structure, is reduced here by 47 % for a wind speed of 30 m/s, by 44 % for 40 m/s and by 34 % for 50 m/s. It should be noted that the wing root bending moment without gusts also increases with increasing wind speed.

As already mentioned in Section III, the deformation of the wing was recorded using the Image Pattern Correlation Technique (IPCT). This also allows to compare the commanded aileron deflections with the deflections measured in the experiment. This is shown in Fig. 7 for the case with U_∞ = 40 m/s and a gust frequency of 9 Hz.

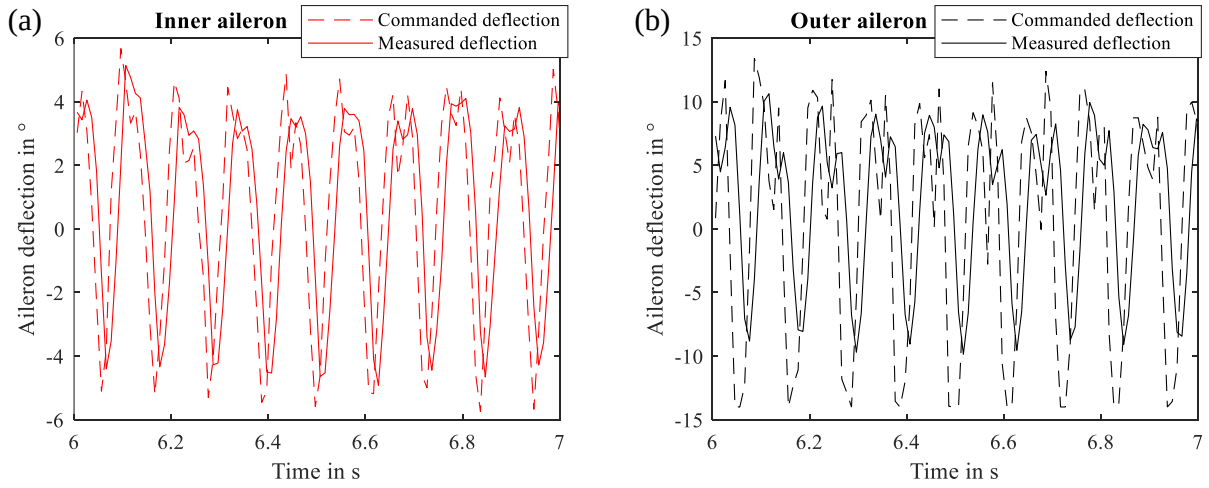

Fig. 7 Comparison of commanded and measured deflection for inner (a) and outer (b) aileron at U_∞ = 40 m/s and f_{gust} = 9 Hz

On the left side of Fig. 7 you can see the courses for the inner aileron and on the right side for the outer aileron. It can be seen that the commanded deflections for the inner aileron are smaller, but the actuator can implement them very well. With the larger deflection commands for the outer aileron, these results are showing that the actuator is not capable to follow with the full amplitude. A delay between the commanded signal and the deflection measured via IPCT can be seen for both ailerons.

Figure 8 shows a case with a wind speed of 50 m/s and a gust frequency of 7 Hz, where the control does not achieve reduction of accelerations. Nevertheless a decrease of the wing root bending moment is visible. It should be noted that in this case, the amplitudes are not as large due to less excitation of the wing and as well the measurement noise has a greater proportion. The reason the accelerations are not reduced here is addressed in Section VI.B by comparing them to the simulative results.

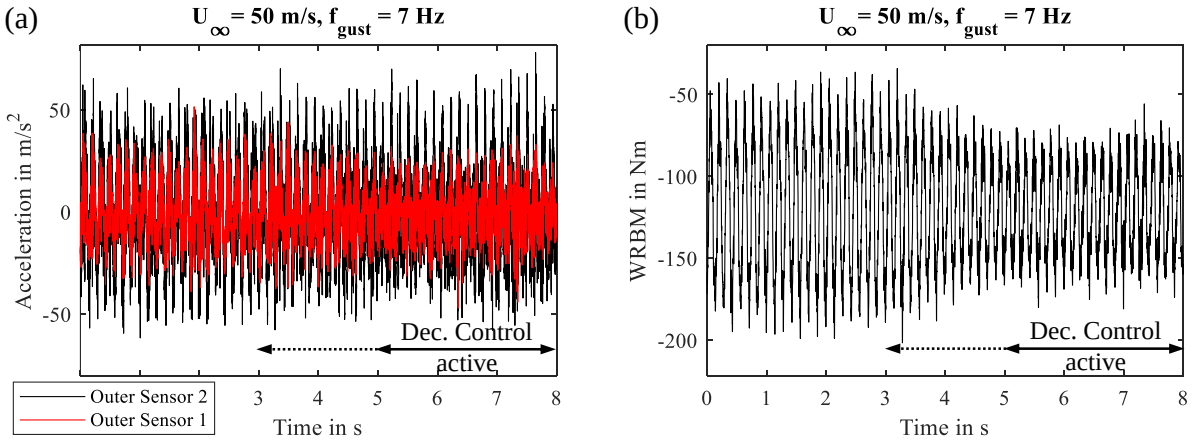

Fig. 8 Acceleration and WRBM measurements at wind speed 50 m/s and gust frequency 7 Hz

Figure 9a shows an evaluation of the maximum accelerations at wind speeds of 30, 40 and 50 m/s and gust frequencies of 3, 7, 9 and 12 Hz. The measuring points with inactive control are shown in blue and those with active control in orange. For clarity, these points are connected with a dotted line. It is easy to see how the accelerations can be highly reduced at a gust frequency of 9 Hz. The maximum acceleration that occurs without control is reduced by 33.6 % by the gust load alleviation control.

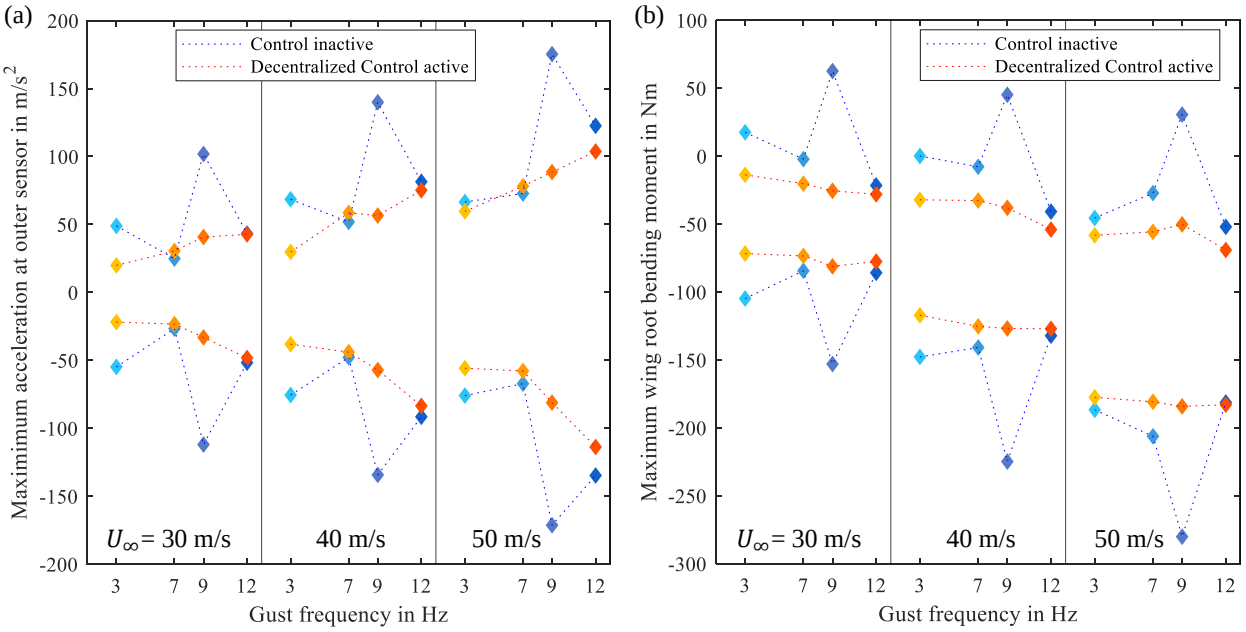

Fig. 9 Envelope of maximum acceleration at outer sensor (a) and maximum WRBM (b) at different wind speeds and gust frequencies

Figure 9b shows the same evaluation for the wing root bending moment. It can be seen that the bending moment is reduced in all areas (with the exception of one measurement point at high speed and gust frequency, where a slight increase occurs). The maximum occurring wing root bending moment with inactive control is reduced by 34.2% by the control.

B. Comparison simulation and wind tunnel results

In a further step, the experimental results are compared with simulative ones. On the one hand, this validates the modeling and, on the other, if experiment and simulation match, unexpected effects that occurred in the experiment can be reproduced.

The input for the simulation is the corresponding measured data from the 5-hole probe in order to reproduce the real gust situation as accurately as possible. The 2-second activation process of the control system is also integrated into the simulation in order to obtain comparable results. In the first instance, the courses of the acceleration of the 'Outer Sensor 2' and the WRBM for a wind speed U_∞ = 50 m/s and a gust frequency of 9 Hz are displayed in Fig. 10. In each case with the course from the simulation in black and the measurements from the experiment in yellow. Here it can be seen that the respective courses are very similar, which indicates the accurate modeling.

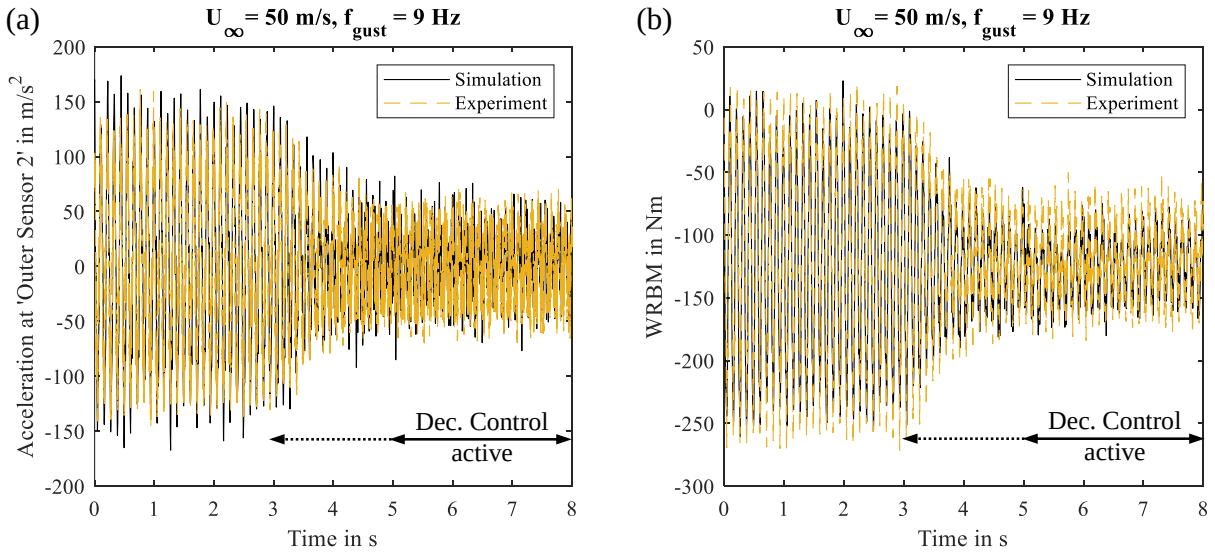

Fig. 10 Simulation with measured gust input vs. experimental measurements at U_∞ = 50 m/s and f_{gust} = 9 Hz

In Section VI.A, it has already been noticed that the accelerations are not reduced at a gust frequency of 7 Hz. In order to understand this, a comparison between simulation and experiment is also performed here. This is shown in Fig. 11 for a wind speed U_∞ = 50 m/s and a gust frequency of 7 Hz. It can be seen that the simulation also shows comparable results with the measured gust input. This is initially good, as it makes it easier to investigate the causes, as the behavior can be reproduced in the simulation.

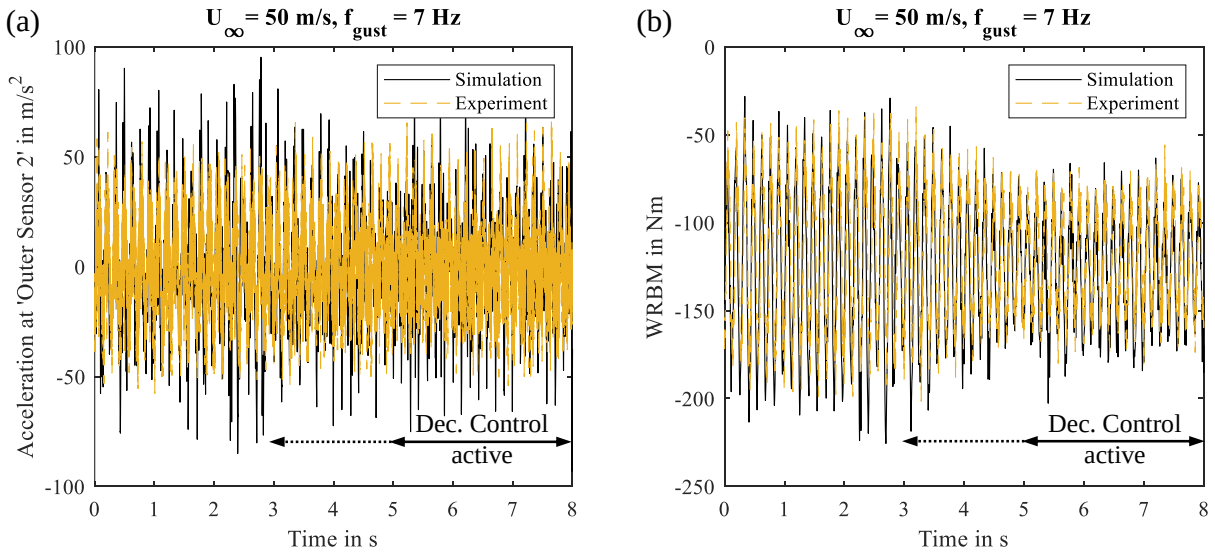

Fig. 11 Simulation with measured gust input vs. experimental measurements at U_∞ = 50 m/s and f_{gust} = 7 Hz

Figure 12 shows the amplitude amplification of a Bode plot of the linear transfer functions from the gust input to the acceleration of the 'Outer Sensor 2'. In the course in blue the control is inactive (open loop), in orange the decentralized control is active (closed loop). Up to 15 Hz there is a strong reduction in the amplitude of the accelerations due to the control. The increases in the higher frequencies are not desirable, but result from the optimization of the controller with 1-cos gusts, which do not have significant amplitudes in this frequency band. Therefore, the increase of magnitude in the high-frequency range was not sufficiently addressed. In the pole-zero plot the displacement of the pole in this high-frequency range shows the reduction of the damping.

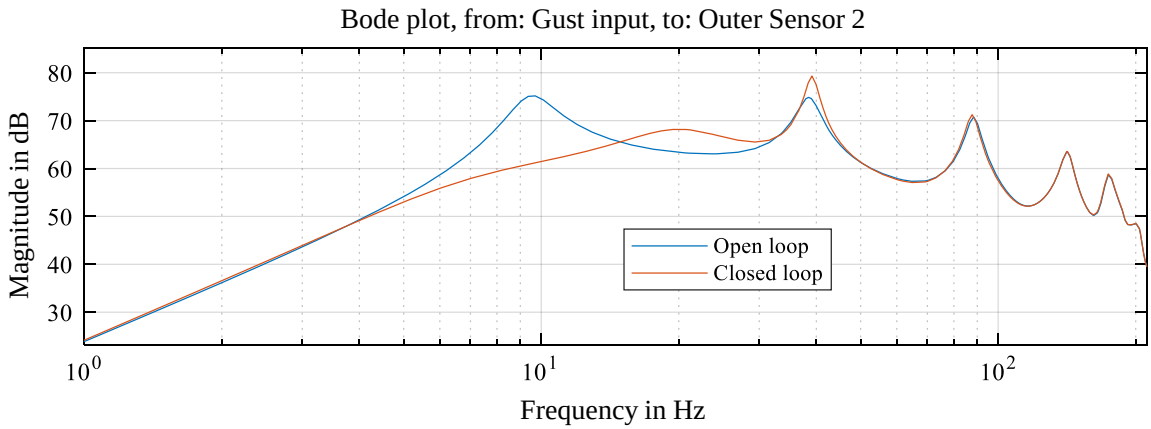

Fig. 12 Amplitude amplification of the open and closed loop linear transfer functions

With a pure sinusoidal 7 Hz gust excitation, a gust load alleviation would therefore also be expected, yet is not observed in the experiment with f_{gust} = 7 Hz. This can be explained by the gust generator's excitation input, which also excites the higher harmonics. In Fig. 13a the amplitude spectrum of the experimental measurement signal of the 5-hole probe can be seen, which was calculated with a Fast Fourier Transformation (FFT). It can be seen here that the excitation at 7 Hz has the greatest amplitude, but multiples of this frequency are also excited. These are not attenuated by the controller, but amplified as seen in Fig. 12. This becomes visible in the amplitude spectrum of the experimental acceleration signal of 'Outer Sensor 2', which is shown in Fig. 13b.

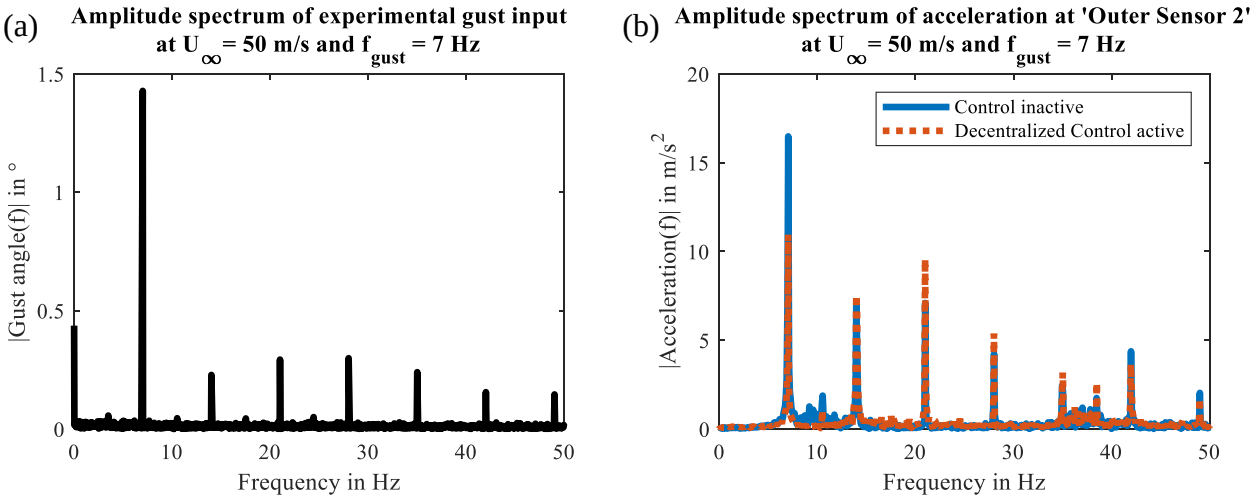

Fig. 13 Amplitude spectrum of gust angle measurement (a) and of acceleration at 'Outer Sensor 2' (b)

The data in Fig. 13b with the control inactive (open loop) is shown in blue, and in orange with active control (closed loop). This shows that the amplitude at 7 Hz is significantly reduced by the control, but the amplitudes particularly at the frequencies 21 and 28 Hz increase. Overall, this results in no reduction of the accelerations at an excitation of 7 Hz with the gust generator. The root bending moment is nevertheless reduced, as can be seen in Fig. 11b.

In the following investigations, it must be considered to what extent gust excitations with a frequency of over 15 Hz can occur in a realistic scenario and what effects this increase of magnitude has there. It may be necessary to work with a low-pass filter with a lower cut-off frequency and/or with a higher order. The resulting phase shift of the filter is expected to reduce the performance in the range of gusts with a frequency component below 15 Hz.

C. Discrete gust excitation

So far, continuous gusts have been shown, for the generation of which the gust generator is ideally suited due to its design. However, discrete, i.e. individually occurring 1-cos gusts are more realistic and are used in the design of the wing structure and in the calculation of the maximum gust loads. Therefore, the gust generator was also used here to simulate this scenario. For this purpose, the cylinders of the gust generator were only moved by 180° instead of a continuous rotation in order to generate a discrete gust event. Figure 3 shows the continuous gust excitation compared to a discrete gust excitation. There you can see that the discrete gust excitation consists of a short excitation downwards and then upwards (speaking from a normal wing perspective).

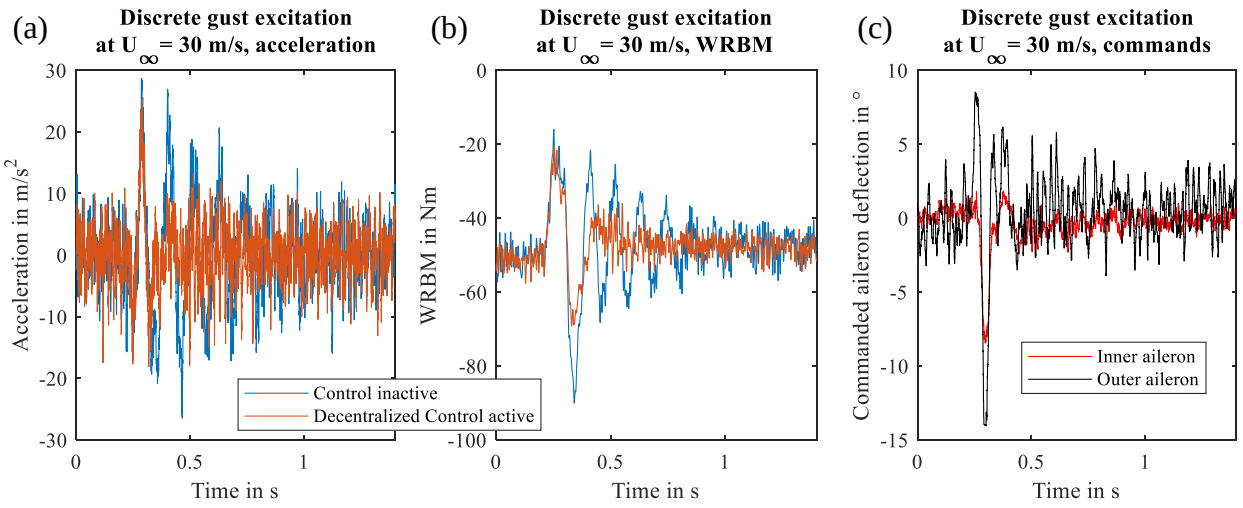

Fig. 14 Evaluation of a discrete gust excitation

In Fig. 14 you can see the wing response to such a discrete gust. Shown here as an example at a wind speed U_∞ = 30 m/s and a targeted rotation frequency of the gust generator of 4.5 Hz. In blue as reference without active GLA control and in orange with active control. Figure 14a shows the acceleration at 'Outer Sensor 2'. The noise of the acceleration values can already be seen before the gust hits (up to approx. 0.2 s). The acceleration at the beginning of the gust can only be slightly mitigated, but particularly the damping of the wing due to the control is easy to recognize. The corresponding plot in Fig. 14b with the wing root bending moment also shows that the deviation of the WRBM from the neutral value is only slightly reduced during the initial downward excitation. With the subsequent upward excitation, which causes an increase in the WRBM (negative sign), a visible reduction in the WRBM is achieved by the control. In particular, the oscillation of the wing, which also manifests itself in an oscillating WRBM, is strongly damped.

Figure 14c shows the commanded control deflections of the two ailerons. The reaction to the accelerations induced by the gust on the wing can be clearly seen. The outer aileron reacts with larger deflections because, on the one hand, the control parameters are slightly larger on the outside, as this aileron is very effective in reducing the gust load. On the other hand, the accelerations on the outer aileron are greater and these are the basis for calculating the control surface deflections in this decentralized concept. Commanded deflections can also be seen before and after the actual gust. These result in part from the excitation by the closed cylinder slot (before and after the discrete excitation), which can also be seen in Fig. 3b. Its excitation with around 25 Hz is not suppressed by the low-pass filter used with a cut-off frequency of 30 Hz. However, lower-frequency noise in the acceleration, which is allowed through by the filter, also leads to this activity in the controller commands. As the actuator has a cut-off frequency of approximately 90 rad/s = 14.3 Hz, not all of these high-frequency commands can be realized. Nevertheless, such activity of the deflection commands is not necessarily desirable, as it leads to increased wear of the actuator. However, when selecting the filter, it should be noted that a filter with a lower cut-off frequency also introduces a higher phase delay in the relevant frequency range (in which you want to react to gusts). This in turn leads to a reduction of control performance, as the delay should be as short as possible with such a feedback control.

To summarize, the experiment shows that a gust load reduction is also achieved with such discrete gust events. However, attention is also drawn to the challenge of filter selection in order to find a compromise between performance and reduction of actuator wear.

VII. Conclusion

The DLR project oLAF offered the opportunity to test the decentralized control for GLA from a flight physical perspective in a wind tunnel. A gust generator was used to induce disturbances on a half-wing equipped with actuated control surfaces. Local control laws were designed and optimized to reduce the gust-induced accelerations by deflecting the respective aileron. With continuous and discrete gust excitations, the wind tunnel experiment demonstrated that the oscillations of the wing are strongly damped. For continuous gusts, it was shown that across different wind speeds and gust frequencies the maximum occurring acceleration is reduced by 33.6 % . The maximum occurring wing root bending moment is reduced by 34.2 %. In particular, it was also shown that comparable gust load alleviation is achieved as with central control approaches [24, 25].

In a following project [26] the decentralized control will be tested in a system test bed with hardware for each component e.g. flight control computer, remote electronic units and full-scale actuators. The interaction between the systems will also be examined in depth there.

Acknowledgments

The wind tunnel experiment took place in the frame of the DLR project oLAF in excellent cooperation between the Institute of Aeroelasticity, the Institute of Aerodynamics and Flow Technology and the Institute of System Dynamics and Control.

The authors would like to thank all contributors to the experiment, particularly Marc Braune, Markus Ritter, Johannes Dillinger, Wolf R. Krüger, Holger Mai, Tania Kirmse, Jan Wagner, Thiemo M. Kier, Martin Tang and Julius Sieg. Here again special thanks to Tania Kirmse for processing and providing the IPCT data. And last but not least thanks to the DNW-NWB team, who made this experiment possible with their active support at the wind tunnel.

References

[1] MacMartin, D., "Collocated structural control: motivation and methodology," *Proceedings of International Conference on Control Applications*, 1995, pp. 1092–1097. https://doi.org/10.1109/CCA.1995.555912.

[2] Michel, K., Schulz, S., Looye, G., and Weber, G., "Decentralized Control of Ailerons for Gust Load Alleviation," *International Forum on Aeroelasticity and Structural Dynamics (IFASD) 2024*, 2024.

[3] Weber, G., Hartmann, A., Schneider, C., Golomazov, V., Wallace, C., Fezans, N., and Kier, T., "Decentralized Load Alleviation System," *SEE MEA (More Electric Aircraft) 2021*, 2021. URL https://elib.dlr.de/146762/.

[4] Wallace, C., Schulz, S., Fezans, N., Kier, T., and Weber, G., "Evaluation Environment for Cascaded and Partly Decentralized Multi-Rate Load Alleviation Controllers," *33rd Congress of the International Council of the Aeronautical Sciences, ICAS 2022*, 2022. URL https://elib.dlr.de/188264/.

[5] Dillinger, J., Mai, H., Krüger, W. R., Schmidt, T. G., and Stalla, J. F., "Design, Manufacturing and Identification of an Actively Controlled Flexible Wing for Subsonic Wind Tunnel Testing," *International Forum on Aeroelasticity and Structural Dynamics, IFASD 2024*, 2024. URL https://elib.dlr.de/205840/.

[6] Schmidt, T. G., Dillinger, J., Ritter, M. R., Altkuckatz, A., Hanke, C., Braune, M., Krüger, W. R., and Mai, H., "Design and Experimental Characterization of a Gust-Generator Concept with Rotating-Slotted Cylinders in the Low-Speed Wind Tunnel DNW-NWB," *International Forum on Aeroelasticity and Structural Dynamics, IFASD 2024*, 2024. URL https://elib.dlr.de/205804/.

[7] Dewetron, "Precision data acquisition systems," , 2024. URL https://www.dewetron.com/, accessed on November 20, 2024.

[8] Jäger Computergesteuerte Messtechnik, "ADwin real-time solutions," , 2024. URL https://www.adwin.de/, accessed on November 26, 2024.

[9] Kirmse, T., Boden, F., Meyer, R., and Philipp, F., "Wing deformation measurements for manoeuvres of high load at the Airbus A320 DLR-ATRA by means of Image Pattern Correlation Technique," *European Test and Telemetry Conference Proceedings Online*, edited by ETTC, 2021, pp. 1–6. URL https://elib.dlr.de/145368/.

[10] Kier, T., and Looye, G., "Unifying Manoeuvre and Gust Loads Analysis Models," *International Forum on Aeroelasticity and Structural Dynamics (IFASD) 2009*, 2009.

[11] Reschke, C., "Integrated Flight Loads Modelling and Analysis for Flexible Transport Aircraft," Ph.D. thesis, University of Stuttgart, Stuttgart, Germany, 2006. https://doi.org/10.18419/opus-3733.

[12] Wright, J. R., and Cooper, J. E., *Introduction to Aircraft Aeroelasticity and Loads*, 2nd ed., Wiley, Chichester, United Kingdom, 2015. https://doi.org/10.1002/9781118700440.

[13] Guyan, R. J., "Reduction of stiffness and mass matrices," *AIAA Journal*, Vol. 3, No. 2, 1965, p. 380. https://doi.org/10.2514/3.2874.

[14] Albano, E., and Rodden, W. P., "A Doublet-Lattice Method for Calculating Lift Distributions on Oscillating Surfaces in Subsonic Flows," *AIAA Journal*, Vol. 7, No. 2, 1969. https://doi.org/10.2514/3.5086.

[15] Blair, M., "A Compilation of the Mathematics Leading to the Doublet Lattice Method," Technical Report, ADA256304, United States Air Force Wright Laboratory, 1992. https://apps.dtic.mil/sti/citations/ADA256304.

[16] Roger, K. L., "Airplane Math Modeling Methods For Active Control Design," *AGARD Conference Proceedings 228*, Advisory Group For Aerospace Research and Development of NATO (AGARD), 1977.

[17] Karpel, M., "Design for Active Flutter Suppression and Gust Alleviation Using State-Space Aeroelastic Modeling," *AIAA Journal*, Vol. 19, No. 3, 1982. https://doi.org/10.2514/3.57379.

[18] Mayo, A., and Antoulas, A. C., "A Framework for the Solution of the Generalized Realization Problem," *Linear Algebra and its Applications*, Vol. 425, 2007. https://doi.org/10.1016/j.laa.2007.03.008.

[19] Antoulas, A. C., Lefteriu, S., and Ionita, A. C., "A Tutorial Introduction to the Loewner Framework for Model Reduction," *Model Reduction and Approximation*, edited by Peter Brenner et al., Society for Industrial and Applied Mathematics (SIAM), Philadelphia, USA, 2017, Chap. 8, pp. 335–376. https://doi.org/10.1137/1.9781611974829.ch8.

[20] European Union Aviation Safety Agency, "Certification Specifications and Acceptable Means of Compliance for Large Aeroplanes (CS-25): CS-25," , 2023.

[21] Stalla, F., et al., "Wind Tunnel Testing Active Gust Load Alleviation on an Experimental Wing," *International Forum on Aeroelasticity and Structural Dynamics (IFASD) 2024*, 2024.

[22] Keviczky, L., Bars, R., Hetthéssy, J., and Bányász, C., *Control Engineering*, Advanced Textbooks in Control and Signal Processing, Springer Nature Singapore, 2019.

[23] Joos, H.-D., Bals, J., Looye, G., Schnepper, K., and Varga, A., "A multi-objective optimisation-based software environment for control systems design," 2002, pp. 7–14. URL https://elib.dlr.de/11882/.

[24] Stalla, F., Looye, G., Kier, T. M., Michel, K., Schmidt, T. G., Hanke, C., Kirmse, T., and Pusch, M., "Wind Tunnel Assessment of a Robust Gust Load Alleviation Controller Designed Using μ-Synthesis," *AIAA SciTech 2025 Forum*, 2025.

[25] Micheli, B., Tang, M., Stalla, F., Hanke, C., Schmidt, T. G., Mai, H., and Krüger, W. R., "Design and Experimental Validation of Gust Load Alleviation Based on $\mathcal{H}$-Optimal Blending of Inputs and Outputs," *AIAA SciTech 2025 Forum*, 2025.

[26] Schumann, H., Lübbe, S. M., Klimmek, T., and Quero, D., "Prüfstand für multifunktionale Flugsteuerungssysteme zur Lastminderung und Flatterunterdrückung bei Verkehrsflugzeugen," *Deutscher Luft- und Raumfahrtkongress 2023*, 2023. URL https://elib.dlr.de/198700/.